# Atom Interferometry with Top-Hat Laser Beams

N. Mielec,[1] M. Altorio,[1] R. Sapam,[1] D. Horville,[2] D. Holleville,[1] L.A. Sidorenkov,[1] A. Landragin,[1] and R. Geiger[1, a)]

[1)] *LNE-SYRTE, Observatoire de Paris, Université PSL, CNRS, Sorbonne Université, 61 Avenue de l'Observatoire, 75014 Paris, France*

[2)] *GEPI, Observatoire de Paris, Université PSL, CNRS, 5 Place Jules Janssen, 92190 Meudon, France*

(Dated: 5 October 2018)

The uniformity of the intensity and phase of laser beams is crucial to high-performance atom interferometers. Inhomogeneities in the laser intensity profile cause contrast reductions and systematic effects in interferometers operated with atom sources at micro-Kelvin temperatures, and detrimental diffraction phase shifts in interferometers using large momentum transfer beam splitters. We report on the implementation of a so-called top-hat laser beam in a long-interrogation-time cold-atom interferometer to overcome the issue of the inhomogeneous laser intensity encountered when using Gaussian laser beams. We characterize the intensity and relative phase profiles of the top-hat beam and demonstrate its gain in atom-optics efficiency over a Gaussian beam, in agreement with numerical simulations. We discuss the application of top-hat beams to improve the performance of different architectures of atom interferometers.

Inertial sensors based on light-pulse atom interferometry address various applications ranging from inertial navigation[1–3], metrology[4–6], gravimetry[7–13] and gradiometry[14,15], tests of fundamental physics[16–21], or gravitational wave astronomy[22,23]. Light-pulse atom interferometers rely on the coherent transfer of momentum from the photons of counter-propagating laser beams to free falling atoms in order to split, deflect and recombine the matter-waves. The sensitivity and accuracy of the instruments thus crucially depend on the relative phase uniformity of the laser beams realizing these atom-optics functionalities. State-of-the-art cold-atom sensors typically use sources at few $\mu$K temperatures, interrogation times of several hundreds of milliseconds, and two-photon transitions[5,10,24]. Inhomogeneities in the laser intensity across the atom cloud degrade the atom optics efficiency, which causes a decrease of interferometer contrast and hence a lower signal to noise ratio, as well as systematic effects[25]. Such detrimental effects are amplified in interferometers employing large momentum transfer (LMT) techniques (in which several momenta are transferred to the atoms)[21,26], in particular because of diffraction phase shifts[27]. The problem of intensity inhomogeneity can be mitigated by employing Gaussian beams with a size much larger than that of the atom cloud, at the cost of a reduced peak intensity.

In this work, we report on the implementation of a *collimated* top-hat laser beam (i.e. with a uniform intensity distribution in the central part[28]) as a solution to circumvent the problems encountered in atom interferometers employing Gaussian beams.

Beamshaping is a topic of intense development, with applications ranging from micro-lithography, optical data storage, or optical tweezers, where different approaches are followed to produce structured light patterns. For application to atom interferometry, the requirement on the relative phase homogeneity motivates a scheme where the counter-propagating beam pair is obtained by retro-reflection (the retro-distance typically lying in the ten-centimeters-to-meter scale). The interrogation laser beams are thus required to be well collimated over such distances. This requirement on the beam shaping technique amounts to achieving a flat phase profile.

The simplest form of shaping the intensity distribution of a laser beam, apodization, results in significant loss of optical power (for example, the optimal transformation of a Gaussian beam into a beam with a flat intensity profile sacrifies 64% of the power). More efficient techniques involve diffractive optical elements, such as spatial light modulators (SLMs), in order to produce focused light patterns[29], or collimated structured beams when multiple SLMs are cascaded[30]. However, the bulkiness of the optical setup, the potential drift of the beam-shaping performance linked to the use of an active material, and the limited incident peak intensity make such solutions cumbersome for atom interferometry experiment. Instead, passive refractive techniques based on aspheric optical elements[31] seem favorable, owing to their compactness, stability, and efficiency.

Our passive top-hat collimator solution is based on a recently released commercial beamshaper from the Asphericon company (model TSM-25-10-S-B), see Fig. 1a). The beamshaper shall receive at its input a Gaussian beam of 10 mm $1/e^2$-diameter and produce a top-hat beam of 15 mm full width at half maximum (FWHM), with a region of about 14 mm where the intensity varies by less than 10% (Ref.[32]). The beamshaping is done with multiple aspheric optics, based on principles similar to those of Ref.[31]. The advertized uniformity of intensity plateau is 0.056 rms, with a phase inhomogeneity of $\lambda/3$ peak-valley (PV) and $\sim \lambda/20$ rms, allowing the beam to propagate without deformation on distances of several meters[32]. We inject the beamshaper with a home-made fiber collimator made of 3 simple lenses, to produce a

[a)] Electronic mail: remi.geiger@obspm.fr

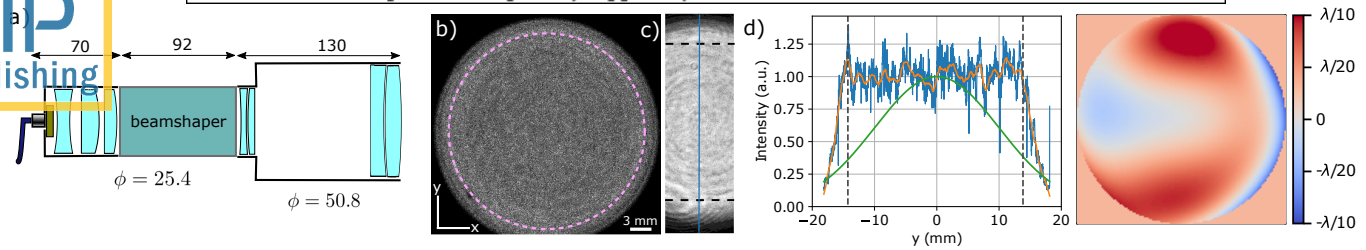


FIG. 1. a) Schematic view of the optical system with the input collimator, the beamshaper, and the expander (dimensions in mm, $\phi$ denoting the diameter of the optics). b) Image of the top-hat beam on a paper screen. The dashed purple line is a circle of 28 mm diameter. c) Image obtained with a beamprofiler, after 40 cm of propagation. Between the 2 dashed lines separated by 28 mm, the uniformity of the plateau is 0.11 rms. d) (blue) Vertical line profile of the top-hat beam shown in c); the intensity has been normalized to the mean plateau intensity. (orange) Moving average over 1 mm. (green) Theoretical profile of a Gaussian beam with 40 mm $1/e^2$ diameter. e) Relative phase of the top-hat beam with 70 cm propagation difference, in a disk of 28 mm; the deviation is $\lambda/5$ (PV) and $\lambda/28$ (rms).

Gaussian beam of $9.95 \pm 0.05$ mm $1/e^2$ diameter. At the output of the beamshaper, the top-hat beam is magnified by a factor of two with two achromatic doublets, in order to reach a useful region of 28 mm. The optical system can be mounted conveniently on an experiment. The power transmission of the input collimator plus the beamshaper is 91%, while that of the full system is 85%. The quality of the generated top-hat beam mainly depends on the input beam size (which must fall within the 10 mm diameter specification at the 10% level[32]), and of its collimation.

To align the top-hat collimator, we image the beam on a paper screen, and optimize the intensity profile by moving the input fiber placed on a 5-axis mount. We target a flat circular intensity profile maintained over a propagation distance of at least 150 cm. Fig 1b) shows the beam imaged on the paper screen at the output of the expander. While this method is convenient for the alignment procedure, it is not suited for a precise measurement of the intensity uniformity of the beam because of the speckle produced on the paper screen. We use a large-area beamprofiler ($11.3 \times 6.0$ mm$^2$) to measure the uniformity of the plateau. Fig 1c) shows the stitched images acquired by scanning the beamprofiler in front of the beam after 40 cm of propagation. The beam exhibits a qualitatively flat plateau. Large diameter rings concentric to the beam are attributed to the beamshaper. The uniformity of the plateau over a diameter of 28 mm is 0.11 rms, and the FWHM is $31.7 \pm 0.2$ mm. Fig 1d) shows a profile of the vertical cut through the middle of the beam (along the blue line). The orange line is a moving average over 1 mm of the profile, shown here to illustrate lower frequency inhomogeneities. For comparison, the green line shows a Gaussian beam with 40 mm diameter at $1/e^2$ (as used in Ref.[24]) and same peak intensity as the top-hat beam.

In an atom interferometer, the relative phase between two counter-propagating laser beams is imprinted on the atomic wave-function during the light pulses. This relative phase contains a term associated with the free propagation, $\varphi(x, y, 0) - \varphi(x, y, 2L)$, where $L$ the distance between the atom cloud and the retro-mirror[33]. We measured such relative phase field for our top-hat beam using an asymmetric Michelson interferometer with the difference of its arms set to $2L$. At the output, the interference pattern carries the 2D relative phase map, which we recover using a Fourier analysis[34]. A lower bound on the accuracy is set by the planeity of the mirrors and of the beamsplitter used in the interferometer, specified to be $\lambda/10$ peak-valley (PV). The relative phase map in a pupil of 28 mm diameter corresponding to the useful part of the beam is shown Fig 1e), for a difference in propagation distance $2L = 70$ cm. We find relative phase inhomogeneities of $\lambda/5$ PV and a $\lambda/28$ rms. Additional phase maps for further propagation distances are given in the supplemental material. Our characterizations show that the top-hat beam is suitable for high-precision atom interferometry, where relative wavefront inhomogeneities are an issue[13,25,33,35].

We implemented the top-hat beam on a cold-atom gyroscope-accelerometer experiment. The setup has been described in previous works[24,36] and we recall here the main features which are relevant for this study. Laser-cooled Cesium atoms (temperature of 1.2 $\mu$K) are launched vertically with a velocity of up to 5.0 m.s$^{-1}$. After a selection step of the $m_F = 0$ magnetic sublevel, we realize the atom interferometer by means of two-photon stimulated Raman transitions from counter-propagating laser beams, which couple the $|F = 3, m_F = 0\rangle$ and $|F = 4, m_F = 0\rangle$ clock states. The direction of the Raman beams is nearly horizontal. We use two beams separated vertically by a distance of 211 mm. The top-hat collimator was set up at the position of the top beam, while the bottom beam is a Gaussian beam of 40 mm diameter at $1/e^2$ (Fig. 2a)). The state of the atoms at the output of the interferometer is finally read out using fluorescence detection.

We first probe the intensity profile of the top-hat beam by applying a Raman pulse of fixed duration $\tau$ at different times as the atoms travel on their way up. The atoms are launched with velocity of 4.7 m.s$^{-1}$, and their mean trajectory intersects the center of the beam after a time of

flight (TOF) of 170 ms. After this relatively short TOF, the size of the cloud is still close to that of the initially launched atoms ($\simeq 1.5$ mm rms radius) and much smaller than the beam size. The transition probability, $P \propto \sin^2(\Omega(z)\tau/2)$, is determined by the local value of the two-photon Rabi frequency, $\Omega(z)$, and can thus be used as a probe of the local intensity of the beam (here $z$ denotes the direction parallel to gravity). Fig. 2b) shows the transition probability versus the relative position of the cloud inside the beam. We observe a qualitatively flat intensity profile in the center, with a width consistent with the optical characterization reported in Fig. 1.

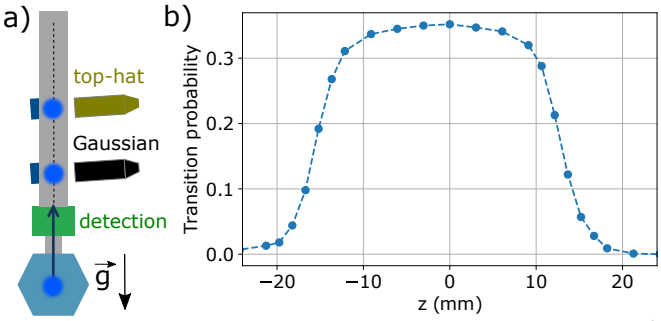


FIG. 2. a) Sketch of the experiment. b) Measurement of the local Raman lasers intensity with a cold atom cloud, by recording the transition probability versus time-of-flight. The duration of the Raman pulse is fixed ($\tau = 9$ $\mu$s) and set close to that of a $\pi/2$ pulse, where the sensitivity to intensity fluctuations on the plateau is maximum. The horizontal axis ($z$) is obtained by multiplying the TOF with the mean velocity of the atoms in the beam (3.0 m.s$^{-1}$).

The size of a cold atom cloud increases over free propagation due to finite temperature. This results in an inhomogeneous atom-light coupling when the cloud size approaches the waist of the Gaussian beam, thereby decreasing the interferometer contrast. The intensity homogeneity of the top-hat beam allows in principle to improve on this effect. To illustrate this improvement, we operate a 3 light-pulse interferometer sequence with a pulse separation time $T = 1$ ms, after a long TOF of 855 ms to bring forward the effect of the atom cloud expansion. For a quantitative comparison, the difference in height between the two beams (211 mm) was matched by the respective change in launch velocity, in order to obtain nearly the same TOFs when crossing the Gaussian and top-hat beams. Fig. 3 presents the comparison and shows the advantage of the top-hat beam.

To assess the limitations to the gain in atom-optics efficiency offered by our top-hat beam over our Gaussian beam, we recorded Rabi oscillations after various TOF, when the launched atom cloud crosses the beams on its way up and on its way down. Fig 4a) shows the Rabi oscillations on the way up after a TOF of 170 ms and on the way down after TOF of 855 ms for the top-hat and Gaussian beams. On the way up, the cloud size is smaller than the beam sizes, and the Rabi oscillations have a similar shape for the Gaussian and top-hat beams, as expected.

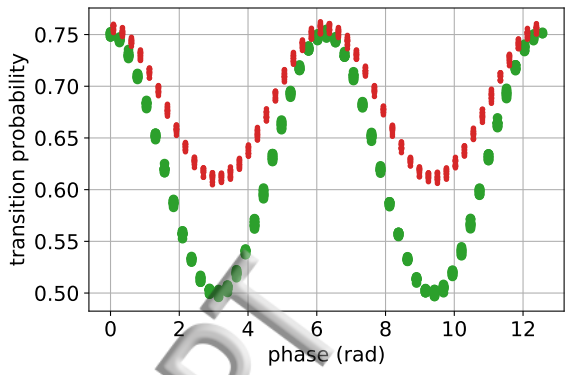


FIG. 3. Interference fringes for a 3-pulse interferometer sequence with a pulse separation time $T = 1$ ms, after a TOF of 855 ms. Red: Gaussian beam. Green: top-hat beam. The interference fringes are scanned by varying the relative Raman laser phase at the third light pulse. The same optical power was used for the Gaussian and the top-hat beams.

The transfer efficiency of $\sim 70\%$ is limited by the velocity selectivity of the two-photon transition, given by the finite Rabi frequency (i.e. laser power) and velocity spread of the atoms in the direction of the beams. On the contrary, on the way down, the Rabi oscillation in the top-hat beam (green) is significantly improved with respect to that in the Gaussian beam (red), owing to the homogeneity of the two-photon Rabi frequency from the top-hat beam. To model the Rabi oscillations, we employ a Monte-Carlo simulation where we generate an ensemble of atoms with individual velocities following the distribution measured with the Doppler-sensitive Raman transitions (corresponding to a 3D temperature of 1.2 $\mu$K), and propagate them in the Raman beams. The details of the model are given in the Supplementary Material. The model reproduces well the data, and allows to assess the residual intensity inhomogeneities of the top-hat beam. Fig. 4b) shows the measured Rabi oscillation confronted to a simulation where intensity noise of various levels is added on the top-hat profile[37]. The data match best the numerical simulation assuming an inhomogeneity of 8.3% rms, consistent with the optical characterization of the intensity inhomogeneities of 11% reported in Fig. 1.

Finally, we demonstrate that the top-hat beam is suited for high-sensitivity atom interferometry, by running a 3-pulse atom interferometer sequence with a pulse separation time $T = 147$ ms. The first $\pi/2$ pulse is realized in the Gaussian beam (on the way up, TOF = 170 ms), while the second and third pulses are realized in the top-hat beam (TOF = 317 and 464 ms). For such long interrogation time, the interferometer is highly sensitive to vibration noise producing at its output a typical rms phase shift of more than $\pi$ rad. Running the interferometer results in a random sampling of the fringe pattern by vibration noise, which appears blurred without additional knowledge on vibration noise at each run. To extract the contrast, we follow the method of Ref.[2]

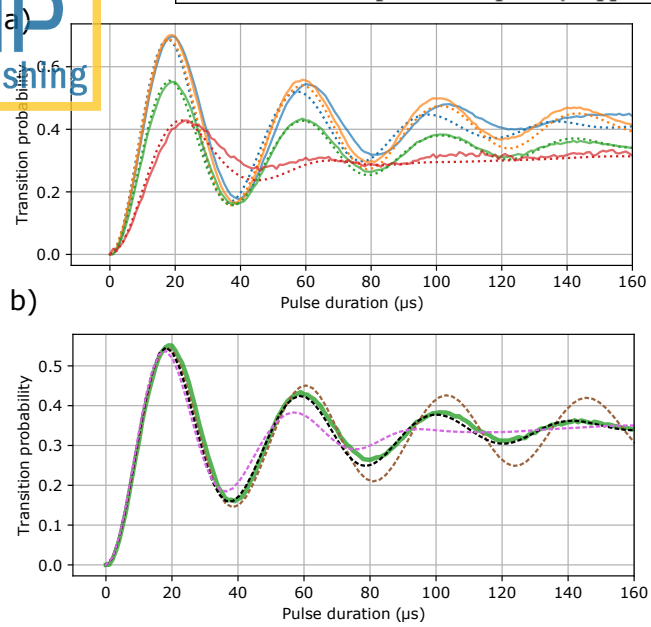


FIG. 4. Rabi oscillations. a) Plain lines: measured oscillations on the way up after 170 ms of TOF (blue and orange for Gaussian and top-hat, respectively), and on the way down after 855 ms of TOF (red and green). Dotted lines: numerical simulation. b) Green plain line: measured Rabi oscillation in the top-hat beam after 855 ms of TOF (the same as in a)). Dashed: numerical simulation for various level of rms intensity noise on the top-hat (brown: 0%, black: 8.3%, violet: 15%).

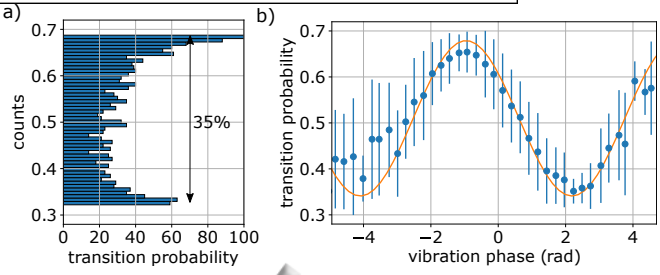


FIG. 5. Performance of the 3-pulse interferometer with $2T = 294$ ms. a) Histogram of the transition probability showing a contrast of 35%. b) Transition probability versus the vibration phase calculated from the data of a broadband seismometer. The data points are sorted along the x-axis and binned in intervals of 262 mrad width. The imperfect estimation of the vibration phase by the seismometer translates into phase noise and consequently into probability noise when binning. Error bars denote 1 standard deviation. The orange plain curve shows a sinusoidal fit where the fringe amplitude is set to the value of 35% extracted from a).

and compute the histogram of the transition probability data (Fig. 5a), from which we extract a contrast of 35%. Furthermore, we recover the interference fringes by correlating the atom interferometer output with the phase calculated from vibration data acquired with two brodband seismometers[24,38], see Fig. 5b). The uncertainty ($1\sigma$) on the fitted phase is 80 mrad, corresponding to an horizontal acceleration uncertainty of $2.5 \times 10^{-7}$ m.s$^{-2}$. Although the measurement sensitivity is limited by residual vibration noise, this experiment shows that the top-hat beam is compatible with high-sensitivity inertial measurements based on long-interrogation-time cold-atom interferometry.

In conclusion, we have set up and characterized a collimated top-hat laser beam and reported on its implementation in a long interrogation time cold-atom interferometer. Our top-hat beam features a constant intensity over a region of 28 mm with rms variations of about 10%, We expect that the intensity homogeneity offered by top-hat beams compared to Gaussian beams will be beneficial to various atom interferometer geometries which we discuss below. We present additional advantages in the Supplementary Material.

The intensity homogeneity of the interrogation beams will allow reducing or canceling important systematic effects in cold-atom interferometers, such as the two photon light shift[39]. It can also be used to improve the efficiency and stability of atom launching techniques based on the coherent transfer of photon momenta, such as in Bloch oscillations[4,6,21]. Moreover, this beamshaping solution could be adapted for atom interferometers with baselines of several meters as in Ref.[21].

Employing a single top-hat beam can be used to build compact, yet precise, cold-atom inertial sensors. For example, a $D = 28$ mm wide homogeneous intensity profile should allow to run a fountain interferometer with a total interferometer time $2T \simeq 2 \times \sqrt{2D/g} = 151$ ms if the atoms are launched from the bottom of the beam. Moreover, the design of gyroscopes, where the atoms travel through successive laser beams with a velocity transverse to the momentum transfers[25,40,41], could be simplified with a single top-hat beam.

Homogeneity of the intensity profile should reduce the diffraction phase shifts encountered in LMT Bragg diffraction[42–44]. For example, a variation of 1% of laser intensity in $4\hbar k$ Bragg diffraction amounts to a variation in diffraction phase of about 84 mrad[27]. The rms intensity uniformity of our top-hat beam is between 8% and 11% over a region of 28 mm (Fig. 1c). Keeping a 10% rms intensity variation within a Gaussian beam requires to work within a reduced portion around the center, which translates in using only 25% of the total power. This suggests that the efficiency and accuracy of LMT beam splitters should be significantly improved by employing top-hat beams.

## SUPPLEMENTARY MATERIAL

The Supplementary Material contains additional data showing the intensity profiles (Fig. S1) and relative phase maps (Fig. S2) for various propagation distances, presents the impact of relative phase inhomogeneities on

the atom interferometer bias, explains the details of the model of the Rabi oscillations, and provides numerical examples of the gain in contrast with top-hat beams compared to Gaussian beams for specific interferometer geometries.

## ACKNOWLEDGMENTS

We thank Josiane Firminy and Faouzi Boussaha for their realization of engraved aspheric phase plates in an early design of beamshaper conducted in the beginning of this project. This work was supported by Ville de Paris (project HSENS-MWGRAV), FIRST-TF (ANR-10-LABX-48-01), Centre National d'Etudes Saptiales (CNES), Sorbonne Universités (project LORINVACC), Action Spécifique du CNRS Gravitation, Références, Astronomie et Métrologie (GRAM), and by the European Union's Horizon 2020 research and innovation programme under the Marie Sklodowska-Curie grant agreement No 660081. We thank Laurence Pruvost for fruitful discussions.

[1] B. Canuel, F. Leduc, D. Holleville, A. Gauguet, J. Fils, A. Virdis, A. Clairon, N. Dimarcq, C. J. Bordé, A. Landragin, and P. Bouyer, Phys. Rev. Lett. **97**, 010402 (2006).
[2] R. Geiger, V. Ménoret, G. Stern, N. Zahzam, P. Cheinet, B. Battelier, A. Villing, F. Moron, M. Lours, Y. Bidel, A. Bresson, A. Landragin, and P. Bouyer, Nature Communications **2**, 474 (2011).
[3] P. Cheiney, L. Fouché, S. Templier, F. Napolitano, B. Battelier, P. Bouyer, and B. Barrett, ArXiv e-prints (2018), arXiv:1805.06198 [physics.atom-ph].
[4] R. Bouchendira, P. Cladé, S. Guellati-Khlifa, F. Nez, and F. Biraben, Physical Review Letters **106** (2011), 10.1103/PhysRevLett.106.080801.
[5] G. Rosi, F. Sorrentino, L. Cacciapuoti, M. Prevedelli, and G. M. Tino, Nature **510**, 518 (2014).
[6] R. H. Parker, C. Yu, W. Zhong, B. Estey, and H. Müller, Science **360**, 191 (2018), http://science.sciencemag.org/content/360/6385/191.full.pdf.
[7] A. Peters, K. Y. Chung, and S. Chu, Metrologia **38**, 25 (2001).
[8] Z.-K. Hu, B.-L. Sun, X.-C. Duan, M.-K. Zhou, L.-L. Chen, S. Zhan, Q.-Z. Zhang, and J. Luo, Phys. Rev. A **88**, 043610 (2013).
[9] P. Gillot, O. Francis, A. Landragin, F. P. D. Santos, and S. Merlet, Metrologia **51**, L15 (2014).
[10] C. Freier, M. Hauth, V. Schkolnik, B. Leykauf, M. Schilling, H. Wziontek, H.-G. Scherneck, J. Müller, and A. Peters, J. Phys. Conf. Ser. **723**, 012050 (2016).
[11] S.-K. Wang, Y. Zhao, W. Zhuang, T.-C. Li, S.-Q. Wu, J.-Y. Feng, and C.-J. Li, Metrologia **55**, 360 (2018).
[12] Y. Bidel, N. Zahzam, C. Blanchard, A. Bonnin, M. Cadoret, A. Bresson, D. Rouxel, and M. F. Lequentrec-Lalancette, Nature Communications **9**, 627 (2018).
[13] R. Karcher, A. Imanaliev, S. Merlet, and F. Pereira dos Santos, ArXiv e-prints (2018), arXiv:1804.04909 [physics.atom-ph].
[14] J. M. McGuirk, G. T. Foster, J. B. Fixler, M. J. Snadden, and M. A. Kasevich, Physical Review A **65** (2002), 10.1103/PhysRevA.65.033608.
[15] F. Sorrentino, A. Bertoldi, Q. Bodart, L. Cacciapuoti, M. de Angelis, Y.-H. Lien, M. Prevedelli, G. Rosi, and G. M. Tino, Applied Physics Letters **101**, 114106 (2012).
[16] S. Dimopoulos, P. W. Graham, J. M. Hogan, and M. A. Kasevich, Phys. Rev. Lett. **98**, 111102 (2007).
[17] S. Lepoutre, A. Gauguet, G. Trénec, M. Büchner, and J. Vigué, Phys. Rev. Lett. **109**, 120404 (2012).
[18] D. N. Aguilera, H. Ahlers, B. Battelier, A. Bawamia, A. Bertoldi, R. Bondarescu, K. Bongs, P. Bouyer, C. Braxmaier, L. Cacciapuoti, and et al, Classical and Quantum Gravity **31**, 115010 (2014).
[19] L. Zhou, S. Long, B. Tang, X. Chen, F. Gao, W. Peng, W. Duan, J. Zhong, Z. Xiong, J. Wang, Y. Zhang, and M. Zhan, Physical Review Letters **115** (2015), 10.1103/PhysRevLett.115.013004.
[20] M. Jaffe, P. Haslinger, V. Xu, P. Hamilton, A. Upadhye, B. Elder, J. Khoury, and H. Mller, Nature Physics **13**, 938 (2017).
[21] P. Asenbaum, C. Overstreet, T. Kovachy, D. D. Brown, J. M. Hogan, and M. A. Kasevich, Physical Review Letters **118** (2017), 10.1103/PhysRevLett.118.183602.
[22] W. Chaibi, R. Geiger, B. Canuel, A. Bertoldi, A. Landragin, and P. Bouyer, Physical Review D **93** (2016), 10.1103/PhysRevD.93.021101.
[23] J. M. Hogan and M. A. Kasevich, Phys. Rev. A **94**, 033632 (2016).
[24] I. Dutta, D. Savoie, B. Fang, B. Venon, C. Garrido Alzar, R. Geiger, and A. Landragin, Physical Review Letters **116** (2016), 10.1103/PhysRevLett.116.183003.
[25] A. Gauguet, B. Canuel, T. Lévèque, W. Chaibi, and A. Landragin, Phys. Rev. A **80**, 063604 (2009).
[26] T. Mazzoni, X. Zhang, R. Del Aguila, L. Salvi, N. Poli, and G. M. Tino, Phys. Rev. A **92**, 053619 (2015).
[27] M. Büchner, R. Delhuille, A. Miffre, C. Robilliard, J. Vigué, and C. Champenois, Phys. Rev. A **68**, 013607 (2003).
[28] F. Gori, Optics Communications **107**, 335 (1994).
[29] V. Pal, C. Tradonsky, R. Chriki, N. Kaplan, A. Brodsky, M. Attia, N. Davidson, and A. A. Friesem, Appl. Opt. **57**, 4583 (2018).
[30] H. Ma, Z. Liu, P. Zhou, X. Wang, Y. Ma, and X. Xu, Journal of Optics **12**, 045704 (2010).
[31] J. A. Hoffnagle and C. M. Jefferson, Appl. Opt. **39**, 5488 (2000).
[32] Asphericon website, cited 5 October 2018.
[33] A. Louchet-Chauvet, T. Farah, Q. Bodart, A. Clairon, A. Landragin, S. Merlet, and F. P. D. Santos, New Journal of Physics **13**, 065025 (2011).
[34] M. Takeda, H. Ina, and S. Kobayashi, **72**, 156.
[35] V. Schkolnik, B. Leykauf, M. Hauth, C. Freier, and A. Peters, Applied Physics B **120**, 311 (2015).
[36] M. Meunier, I. Dutta, R. Geiger, C. Guerlin, C. L. Garrido Alzar, and A. Landragin, Physical Review A **90** (2014), 10.1103/PhysRevA.90.063633.
[37] We varied the spatial frequencies of the added intensity noise and found no substantial difference in the simulation results as long as the spatial period was smaller than about 1/10 of the beam size. In the simulation reported in Fig. 3, the spatial period of the noise is 1/100 of the beam size.
[38] S. Merlet, J. LeGouët, Q. Bodart, A. Clairon, A. Landragin, F. Pereira Dos Santos, and P. Rouchon, Metrologia **46**, 87 (2009), arXiv:0806.0164 [physics.atom-ph].
[39] A. Gauguet, T. E. Mehlstäubler, T. Lévèque, J. Le Gouët, W. Chaibi, B. Canuel, A. Clairon, F. P. Dos Santos, and A. Landragin, Phys. Rev. A **78**, 043615 (2008).
[40] G. Tackmann, P. Berg, C. Schubert, S. Abend, M. Gilowski, W. Ertmer, and E. M. Rasel, New Journal of Physics **14**, 015002 (2012).
[41] Z.-W. Yao, S.-B. Lu, R.-B. Li, J. Luo, J. Wang, and M.-S. Zhan, Physical Review A **97** (2018), 10.1103/PhysRevA.97.013620.
[42] S.-w. Chiow, T. Kovachy, H.-C. Chien, and M. A. Kasevich, Physical Review Letters **107** (2011), 10.1103/PhysRevLett.107.130403.
[43] P. A. Altin, M. T. Johnsson, V. Negnevitsky, G. R. Dennis, R. P. Anderson, J. E. Debs, S. S. Szigeti, K. S. Hardman, S. Bennetts, G. D. McDonald, L. D. Turner, J. D. Close, and N. P. Robins, New Journal of Physics **15**, 023009 (2013).
[44] B. Estey, C. Yu, H. Müller, P.-C. Kuan, and S.-Y. Lan, Phys. Rev. Lett. **115**, 083002 (2015).

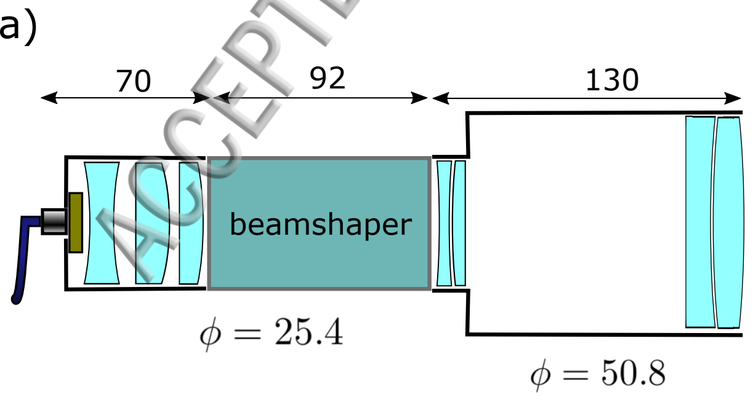
a)
70
92
130
beamshaper
$\phi = 25.4$
$\phi = 50.8$

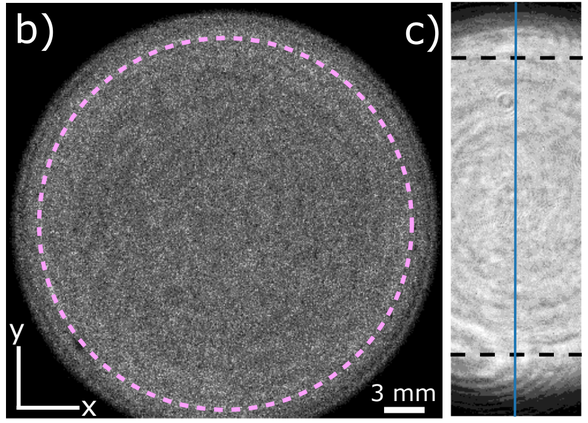
b)
c)
y
x
3 mm

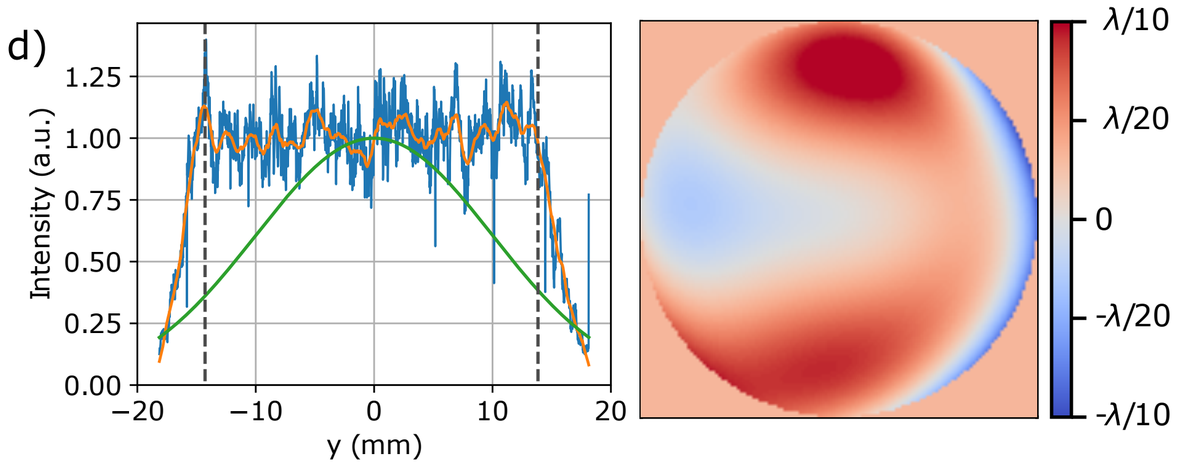
d)
Intensity (a.u.)
1.25
1.00
0.75
0.50
0.25
0.00
−20
−10
0
10
20
y (mm)
λ/10
λ/20
0
-λ/20
-λ/10

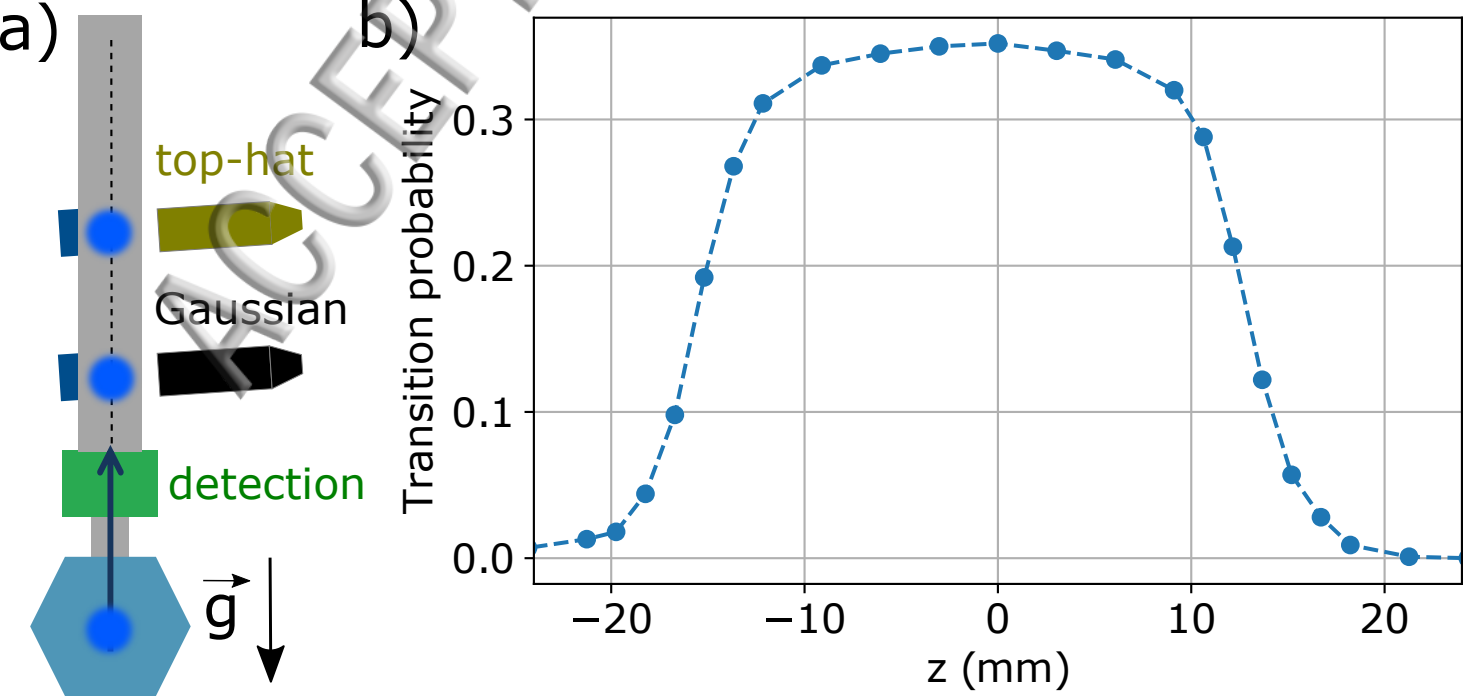
a)
top-hat
Gaussian
detection
$\vec{g}$
b)
Transition probability
0.0
0.1
0.2
0.3
−20
−10
0
10
20
z (mm)

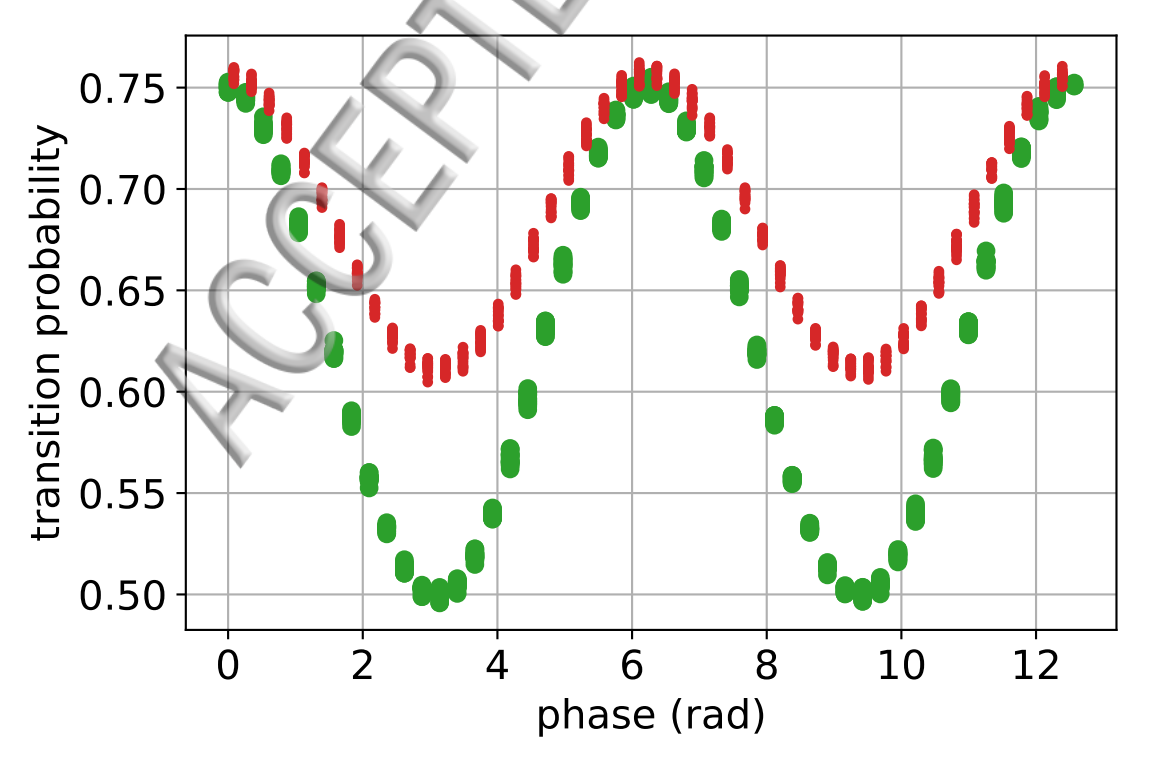
transition probability
0.75
0.70
0.65
0.60
0.55
0.50
0
2
4
6
8
10
12
phase (rad)

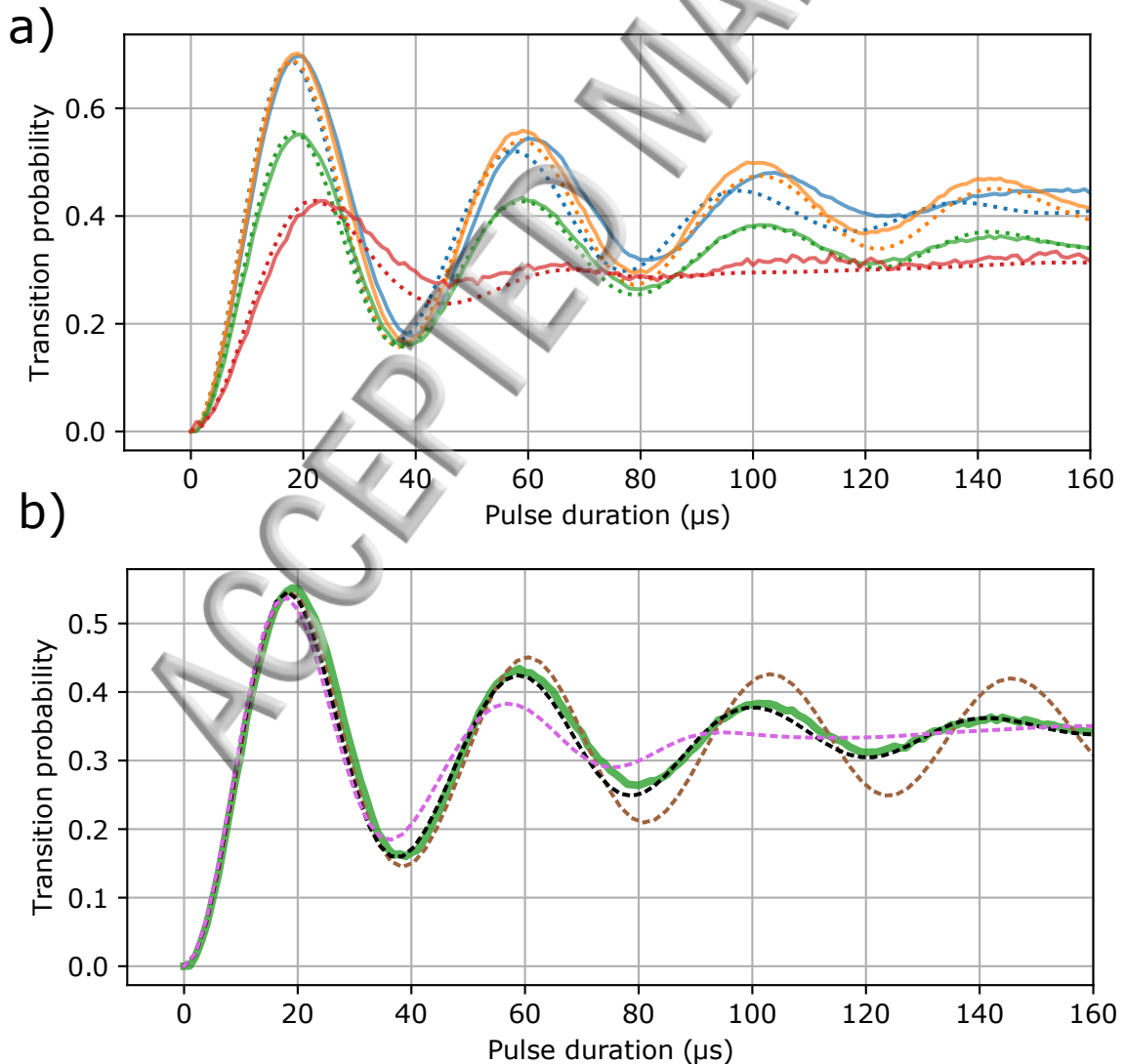
a)
Transition probability
0.0
0.2
0.4
0.6
0
20
40
60
80
100
120
140
160
Pulse duration (μs)
b)
Transition probability
0.0
0.1
0.2
0.3
0.4
0.5
0
20
40
60
80
100
120
140
160
Pulse duration (μs)

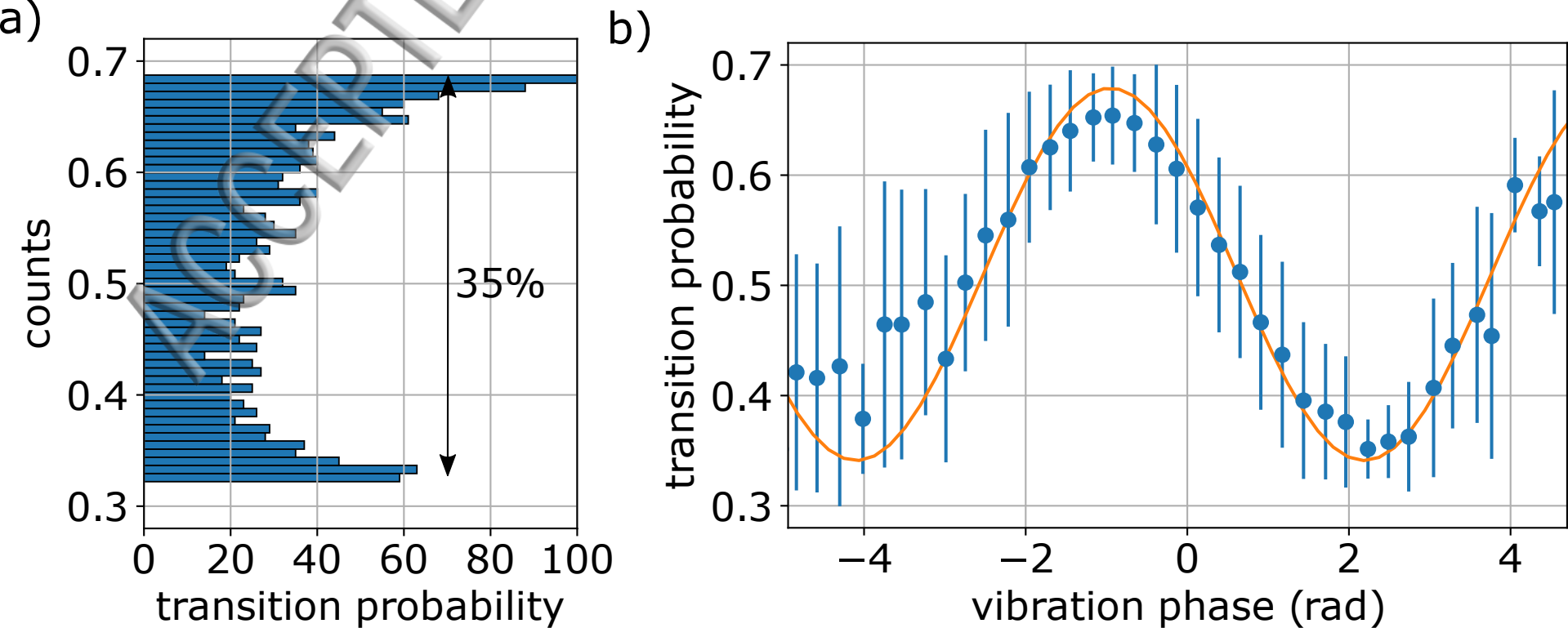
a)
0.7
0.6
0.5
0.4
0.3
counts
35%
0
20
40
60
80
100
transition probability
b)
0.7
0.6
0.5
0.4
0.3
transition probability
−4
−2
0
2
4
vibration phase (rad)